

Real-time dynamics of particle-hole excitations in Mott insulator-metal junctions.

Luis G. G. V. Dias da Silva,^{1,2} Khaled A. Al-Hassanieh,³ Adrian E. Feiguin,⁴ Fernando A. Reboredo,¹ and Elbio Dagotto^{1,2}

¹*Materials Science and Technology Division, Oak Ridge National Laboratory, Oak Ridge, Tennessee 37831*

²*Department of Physics and Astronomy, University of Tennessee, Knoxville, Tennessee 37996*

³*Theoretical Division, Los Alamos National Laboratory, Los Alamos, New Mexico 87545*

⁴*Department of Physics and Astronomy, University of Wyoming, WY 82071, USA*

(Dated: October 24, 2022)

Charge excitations in Mott insulators are distinct from their band-insulator counterparts and they can provide a mechanism for energy harvesting in solar cells based on strongly correlated electronic materials. In this manuscript, we study the real-time dynamics of holon-doublon pairs in a Mott insulator (MI) connected to metallic leads using the time-dependent density matrix renormalization group (DMRG) method. The transfer of charge across the MI-metal interface is controlled by both the electron-electron correlations and the chemical potential difference between the leads, in contrast with the noninteracting case. Moreover, the propagation of holon-doublon excitations within the MI dynamically changes the spin-spin correlations, introducing time-dependent phase shifts in the spin structure factor.

PACS numbers: 71.10.Fd, 71.35.-y

I. INTRODUCTION

The dynamics of excitations in strongly correlated electronic materials (SCEMs)¹ have been the subject of intense study in recent years. In a vast class of SCEMs, the ground state is a Mott insulator (MI), characterized by strong on-site repulsive interactions and a charge gap in the density of states. A paradigmatic model describing this behavior is the one-dimensional (1D) Hubbard model at half-filling, in which elementary charge excitations involve either doubly occupied (doublons) or empty (holons) electronic sites. A doublon-holon pair is thus a charge neutral excitation, which, depending on the relative strength of the on-site and nearest-site repulsion, can either form a bound state (a “Hubbard exciton”) or remain decoupled. These excitonic states in Hubbard-like systems have attracted considerable attention involving both theoretical^{2,3,4} and experimental^{5,6,7} investigations.

A particular framework where the behavior of doubly occupied site excitations has acquired considerable relevance is in experiments involving cold atomic fermionic mixtures in optical lattices.⁸ While these experiments are performed under controlled conditions and allow for a substantial degree of tunability, the ability to properly probe and characterize these systems is limited. A recently proposed technique to probe the spectrum of a Mott insulating state consists of dynamically creating double occupancies by modulating the lattice depth with a time-dependent optical potential.⁹ When the lattice depth exceeds the Mott gap, double occupancy becomes favorable and, by optical methods, it is possible to determine the appearance of the gapped mode.^{10,11} In addition, lattice-modulation spectroscopy has been proposed as a method to detect antiferromagnetic ordering and probe the nature (coherent or incoherent) of quasiparticle excitations.¹² The decay mechanisms associated to the doublon excitations bring up fundamen-

tal questions about thermalization and non-equilibrium dynamics.^{13,14,15}

In addition, technological applications may potentially arise from exploiting charge excitations in Mott insulators as a way to devise SCEM-based solar cells, which can offer structural and optical advantages over current devices made with semiconductor materials. One-dimensional Mott insulators (such as Sr_2CuO_3) are particularly known for strong nonlinear optical response effects^{16,17} that can be exploited in this context. The efficiency of SCEM-based solar cells will depend on several factors, including the performance of Mott-insulator-metal junctions where the photocurrent will be generated. A crucial question is whether charge excitations in the MI will be able to properly transfer the charge into the metallic contacts, thus establishing a steady-state photocurrent.

Several questions arise in these regards: (i) Are the charge excitations long-lived? In other words, what are the effective decaying channels for the holon-doublon excitations into spin excitations inside the MI region? (ii) What are the effects of the dynamics of these excitations on the original correlations in the MI region? (iii) Can these charge excitations propagate across an interface with a non-correlated material?

Point (i) was addressed by some of us in Ref. 18, where the real-time dynamics of a holon-doublon pair was studied in a 1D Mott insulator. In that previous effort it was found that the decay to spin excitations in the underlying spin background is inefficient, and the pair is long-lived. The weak decay to spin-only excitations is particularly telling since the low-lying excitations for the 1D Hubbard model at half-filling carry spin (spinon) and charge (holons) quantum numbers separately and propagate with different characteristic velocities, as described by the Tomonaga-Luttinger liquid picture. The ensuing spin-charge separation of these low-energy modes has

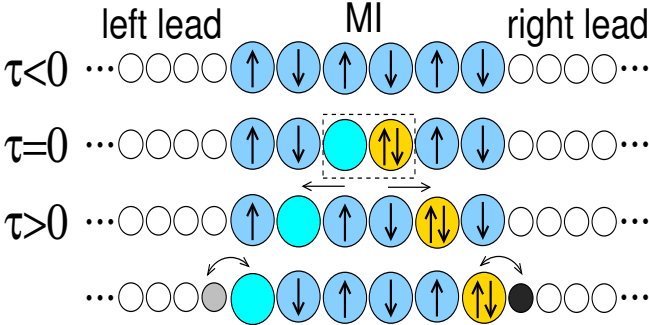


FIG. 1: Schematic representation of the MI+leads system studied here. At time $\tau = 0$, a doublon-holon pair is created at the center of the MI region. This pair propagates and eventually reaches the boundary interface.

been long studied and the real-time dynamics has been explored in recent works.^{19,20}

Points (ii) and (iii) will be addressed in this paper. Here, we study the charge and spin dynamics across a Mott insulator (MI)/metal junction, as doublon-holon excitations are created within the MI. A possible mechanism for such excitations arises from optical absorption at energies of the order of the Mott gap, producing exciton-like states. We study the time evolution of a localized doublon-holon pair initially created within the MI region. We consider a regime with weak nearest-neighbor electron-electron repulsion relative to the kinetic energy within the MI (or, equivalently, weak holon-doublon attraction), leading to a spatial dissociation of the doublon-holon pair, with both excitations eventually reaching the MI-metal boundaries.

The main results are summarized as follows. A strong confinement of the holon-doublon pairs within the MI region occurs for moderate to high values of the on-site interaction U . Nevertheless, charge transmission through the MI-metal boundary can be favored by properly adjusting the chemical potentials in the metallic leads. These dynamic effects strongly influence on the spin-spin correlations within the MI region, effectively reducing the power-law decaying antiferromagnetic (AFM) order and introducing phase shifts in the spin structure factor.

The paper is organized as follows. The model and the details of the calculation are described in Section II. The main results are presented in Sec. III, where we discuss the charge, double occupation and spin-spin correlation dynamics (Sec. III A), as well as compare results against noninteracting cases (Sec. III B). The phase shifts in the spin structure factor are also discussed (Sec. III C). A summary of the main results is given in Sec. IV.

II. MODEL AND METHODS

The metal-MI-metal junction studied here is described by a 1D Hubbard model with on-site and nearest-neighbor Coulomb interaction terms (representing the

MI region) connected to noninteracting sites (representing the metallic leads). The Hamiltonian reads $H = H_{\text{MI}} + H_{\text{leads}} + H_{\text{coupling}}$, with:

$$\begin{aligned}
 H_{\text{MI}} &= -t'' \sum_{\sigma, i=N_L+1}^{N_L+N_{\text{MI}}} c_{i\sigma}^\dagger c_{i+1\sigma} + U \left(n_{i\uparrow} - \frac{1}{2} \right) \left(n_{i\downarrow} - \frac{1}{2} \right) \\
 &\quad + V (n_i - 1) (n_{i+1} - 1) + \text{h.c.} \\
 H_{\text{leads}} &= \sum_{i \in R, L} \mu_{R, L} n_i - t \sum_{\sigma, i \in R, L} c_{i\sigma}^\dagger c_{i+1\sigma} + \text{h.c.} \\
 H_{\text{coupling}} &= -t' \sum_{\sigma, i=N_L; i=N_L+N_{\text{MI}}} \left(c_{i\sigma}^\dagger c_{i+1\sigma} + \text{h.c.} \right) \quad (1)
 \end{aligned}$$

where the sum in H_{coupling} has only two terms ($i = N_L$ and $i = N_L + N_{\text{MI}}$). As standard, $c_{i\sigma}^\dagger$ ($c_{i\sigma}$) represents the creation (destruction) operator of an electron with spin projection σ at site i .

In the model above, H_{MI} describes the central interacting region, with U and V being, respectively, the on-site and nearest-neighbor Coulomb repulsion. t'' is the hopping matrix element between sites in the MI region. The second term (H_{leads}) represents the noninteracting leads, where t is the tight-binding hopping amplitude (taken as the unit of energy hereafter) and μ_ℓ is the chemical potential in lead ℓ . Finally, H_{coupling} describes the coupling between the leads and the MI involving a hopping amplitude t' .

The total length of the 1D chain representing the entire system is $N_L + N_{\text{MI}} + N_R$, where N_L , N_{MI} and N_R correspond to the number of sites in the left lead, Mott insulator, and right lead respectively (referred to as a “ N_L - N_{MI} - N_R configuration”). The key parameters governing the dynamics are the on-site interaction U and the chemical potential difference between the leads, given by $\Delta\mu \equiv (\mu_L - \mu_R)/2$. In the following, we consider symmetric chains with $N_L = N_R = 20$ and $N_{\text{MI}} = 10$ (for a total of 50 sites for the system) and assume a strong lead-MI tunneling amplitude ($t' = t$), which minimizes reflections at the interface due to a hopping matrix mismatch (although reflections due to the fact that $t'' \neq t$ still play a role).

In order to investigate the dynamics of the excitations and tunneling into the metallic leads, we will focus on the regime of weakly bound doublon-holon pairs with negligible recombination probability. Following Ref. 18, these constraints can be met by choosing U and V such that $U/t'' \gtrsim 8$ and $V/t'' \lesssim 0.6$. Thus, here we select the values $t'' = 0.5t$, $V = 0.3t$, and $U > 4$ for our studies. As expressed before, all parameters with units of energy hereafter are given in units of the hopping t .

Figure 1 depicts the metal-MI-metal junction. The equilibrium (“ $\tau < 0$ ”) ground-state $|\psi\rangle_0$ is obtained from static DMRG^{21,22} calculations. At time $\tau = 0$, a doublon-holon pair is suddenly created, by acting with holon (h_i^\dagger) and doublon (d_i^\dagger) creation operators on the

state $|\psi\rangle_0$:

$$|\psi(\tau=0)\rangle = h_p^\dagger d_{p+1}^\dagger |\psi\rangle_0 \quad (2)$$

with $h_i^\dagger \equiv (1/\sqrt{2}) \sum_\sigma c_{i\sigma} (1 - n_{i\bar{\sigma}})$ and $d_i^\dagger \equiv (1/\sqrt{2}) \sum_\sigma c_{i\sigma}^\dagger n_{i\bar{\sigma}}$.

The site where the holon is created is chosen as $p = N_L + N_{\text{MI}}/2$ so that the doublon-holon pair is initially localized at the center of the MI region. This choice, although not crucial, keeps the system symmetric under the application of a particle-hole transformation followed by a reflection through the middle bond.

The real time dynamics is obtained by time-evolving the original state using the time-dependent DMRG method^{23,24} and obtaining $|\psi(\tau)\rangle = e^{-i\hat{H}\tau} |\psi(0)\rangle$. We find that a Suzuki-Trotter decomposition with a time step $\delta\tau = 0.05$ and keeping 200 states during the time evolution provides an adequate choice for time-evolved quantities up to times $\tau \sim 20$. Since the sudden creation of an exciton via Eq. 2 is restricted to only two sites in the original system, we find that, starting from a well converged initial state, increasing the number of states during the time evolution does not significantly alter the main results.

In order to probe the effects of the doublon-holon dynamics on the properties of the system, we calculate the expectation values of local operators \hat{O}_i on site i at each time step. We define the change from the corresponding equilibrium value as $\delta\hat{O}_i(\tau) \equiv \langle\hat{O}_i\rangle(\tau) - \langle\hat{O}_i\rangle_{\text{eq}}$, where $\langle\ldots\rangle$ indicates the expectation value using the time-evolved state $|\psi(\tau)\rangle$ at time τ while $\langle\hat{O}_i\rangle_{\text{eq}}$ is the value calculated at equilibrium ($\tau < 0$). Typical site operators considered here are the on-site charge n_i and double occupation $D_i \equiv d_i^\dagger d_i$.

We also define the “charge transfer” to the right metallic lead as

$$\Delta n_R(\tau, \Delta\mu) \equiv \sum_{i \in R} \langle n_i \rangle(\tau) - \langle n_i \rangle_{\text{eq}} = \sum_{i \in R} \delta n_i(\tau), \quad (3)$$

where the sum runs over sites in the right lead only. This quantity keeps track of the time-integrated charge that is transported into the right lead as a result of the creation of the holon-doublon excitation at $\tau = 0$. A small charge transfer would indicate strong confinement of the doublon-holon pair within the MI region.

We should point out that, as defined in Eq. 2, the doublon is created to the “right” of the holon (i.e., a “left/right” holon-doublon pair), making the right lead the “doublon side” and thus justifying the choice of the right lead for the definition of the charge transfer in Eq. 3. This is only an arbitrary convention since the creation of “left/right” and “right/left” holon-doublon pairs by optical absorption should occur with equal probability. In fact, the effective total charge transfer to the right metallic lead should take into account the contribution from a “right/left” holon-doublon pair as well. Given the symmetries of the system described above, this contribution will be given by $-\Delta n_R(\tau, -\Delta\mu)$ calculated for the

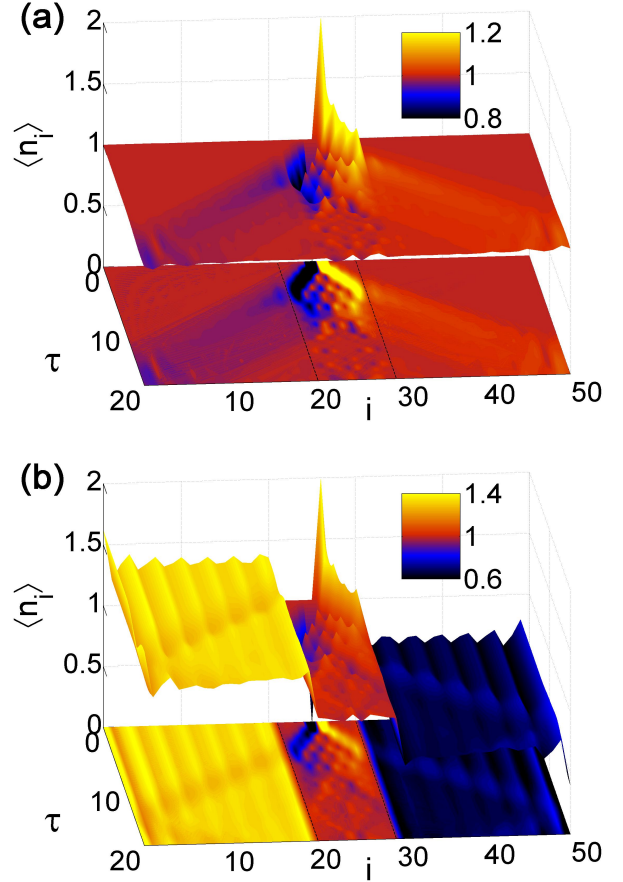


FIG. 2: Charge $\langle n_i \rangle$ on site i versus time τ for a chain with $N = 50$ sites (20-10-20 configuration), using $U = 4$ and (a) $\Delta\mu = 0$ and (b) $\Delta\mu = -1$.

left/right holon-doublon pair. Note that, once this contribution is taken into account, the net current is nonzero only for $\Delta\mu \neq 0$.

Additionally, we investigate the spin-spin correlations away from equilibrium. We calculate the dynamical spin structure factor $S(q, \tau)$, defined as:

$$S(q, \tau) = \frac{1}{N} \sum_{j, k \in \text{MI}} e^{i(j-k)q} \langle S_j^z S_k^z \rangle(\tau), \quad (4)$$

with j, k spanning the interacting region ($j, k \in \text{MI}$). As usual, a peak in $S(q)$ at $q = \pi$ signals quasi-long-range antiferromagnetic order, given in real space by $\langle S_j^i S_{j+k}^i \rangle \sim (-1)^k / r^\alpha$ with α being the critical exponent of the order parameter.

III. RESULTS

A. MI-leads charge transfer

The typical dynamical behavior of the local charge $\langle n_i \rangle(\tau)$ is depicted in Fig. 2-a for $U = 4$ and $\Delta\mu = 0$.

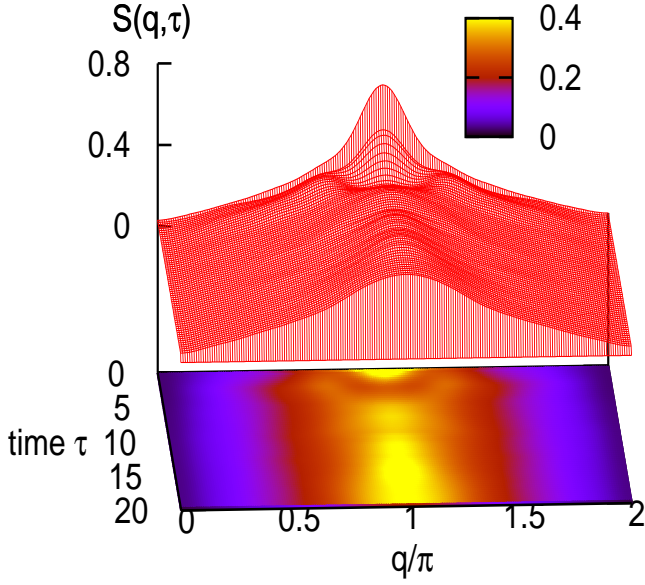


FIG. 3: Spin structure factor $S(q, \tau)$ in the MI region for $U = 4$ and $\Delta\mu = 0$.

At $\tau < 0$, the ground state of the system is particle-hole symmetric, with $\langle n_i \rangle = 1$ for all i . At $\tau = 0$, the doublon-holon pair is created, making $\langle n_p \rangle = 0$, $\langle n_{p+1} \rangle = 2$, and $\langle D_p \rangle = 0$, $\langle D_{p+1} \rangle = 1$ (note that, while the total charge $\sum_i n_i$ is conserved, $\sum_i D_i$ is not constant). Due to the on-site repulsion in the MI, these charge excitations move in opposite directions as a function of τ , eventually reaching the MI-metal interfaces at a time scale $\tau \sim \tau_r$ (for the parameters in Fig. 2, $\tau_r \approx 5.5$).

For a nonzero chemical potential difference between left and right leads, the charge is expected to be non-uniformly distributed, with clear charge “plateaus” in each of the three regions. This is clearly depicted in Fig. 2-b, with $\mu_R > \mu_L$ ($\Delta\mu < 0$). In this case, the equilibrium charge distribution of the system is such that $\langle n_{i \in L} \rangle > 1$, and $\langle n_{i \in R} \rangle < 1$ while $\langle n_{i \in \text{MI}} \rangle \sim 1$ in the MI region. As the doublon excitation approaches the MI-leads boundary, it is then partially transmitted to the right lead while, by symmetry, the holon excitation is partially transmitted to the left lead.

An intuitive picture for such a charge transmission/reflection can be formulated in terms of the single-particle density of states. The energy cost for the formation of the doublon is of the order of the Mott gap, Δ_{MI} . Therefore, from purely energetic considerations, one expects an enhanced transport if there are enough states available in the leads at energies of the order of $\Delta_{\text{MI}}/2$ above the chemical potential in the MI. Static DMRG calculations for the equilibrium density of states (not shown) give Mott gap values $\Delta_{\text{MI}} \approx 2$ for $U = 4$ and $\Delta_{\text{MI}} \approx 8$ for $U = 10$, which is of the order or larger than the typical half bandwidth $\sim 2t$ of the noninteracting

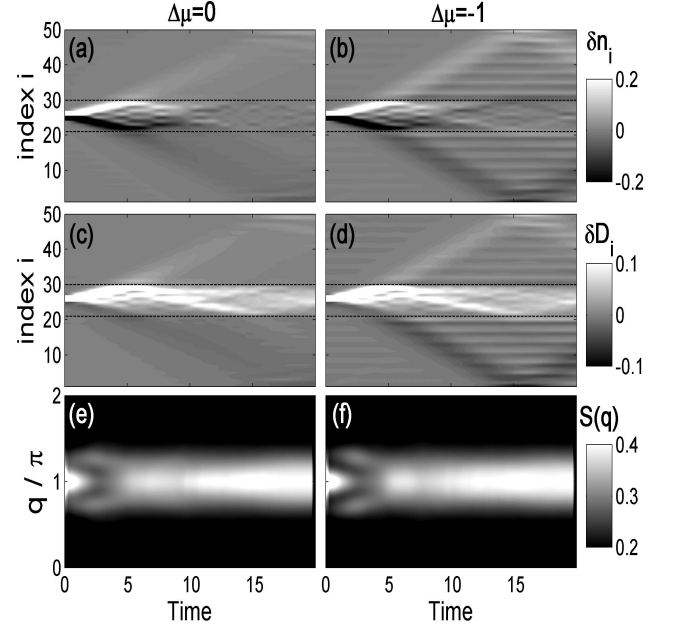


FIG. 4: Nonequilibrium charge difference δn_i (a,c), double occupation δD_i on each site, and spin structure factor $S(q, \tau)$ in the MI region (e,f) versus time. The results are for $U = 4$ with different chemical potentials in the leads: $\Delta\mu = 0$ (a,c,d) and $\Delta\mu = -1$ (b,d,f). Note the pronounced charge transfer for $\Delta\mu = -1$.

chain. Therefore, for $\Delta\mu = 0$ (chemical potentials in the metal and in the MI aligned), one expects a decreasing charge transfer with increasing U . On the other hand, a shift of the chemical potential in the leads should increase the charge transfer thereby allowing a “matching” of states available for $|\Delta\mu| \sim \Delta_{\text{MI}}/2$.

In fact, the reflection at the boundary can be reduced by changing the equilibrium chemical potential in the leads, as shown in Fig. 2-b. In this case, the Fermi energy in the leads is aligned with the band, creating states available for the excitation to “leak” into the leads.

This simplified picture, however, does not take into account the existing correlation effects within the Mott insulator region. Additional insight on the effect of the doublon-holon dynamics can be provided by the spin-spin correlations within the MI region, via the spin structure factor. Fig. 3 shows the time evolution for $S(q, \tau)$ calculated within the interacting (MI) region for $U = 4$. In equilibrium (“ $\tau < 0$ ”, shown as the first curve), a pronounced peak is observed at $q = \pi$ in both cases, signaling AFM correlations. At intermediate times, this peak acquires “shoulders” which become more prominent around $\tau \sim \tau_r/2$, which coincides with the time scale for which the doublon-holon pair is spatially separated but has not yet reached the boundary. For longer times, the peak is broadened, indicating a weaker AFM order within the MI region. We discuss the microscopic mechanisms leading to these interesting dynamical effects in Sec. III C.

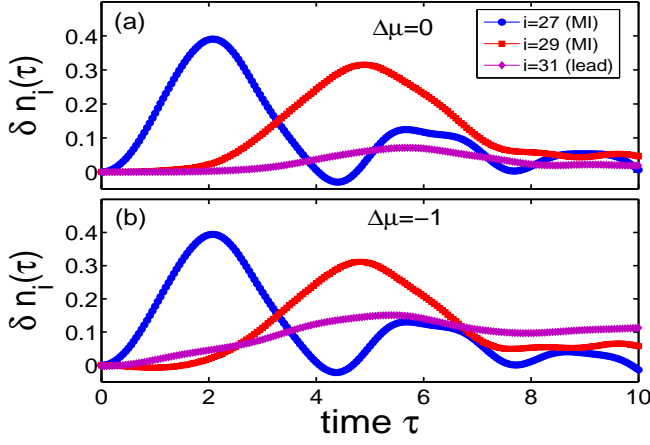


FIG. 5: Charge difference $\delta n_i(\tau)$ on sites near the MI-metal boundary as a function of time for $U = 4$ and (a) $\Delta\mu = 0$ and (b) $\Delta\mu = -1$.

Figure 4 presents a visual summary of the dynamics of the charge, double occupation, and spin-spin correlations for $U = 4$ and different chemical potential differences $\Delta\mu$. Figs. 4 a-b show $\delta n_i(\tau)$ in all sites for $\Delta\mu = 0$ and $\Delta\mu = -1$, respectively. An enhanced charge transmission into the leads is clearly seen for $\Delta\mu = -1$, consistent with the arguments given above. This additional charge is an effect of the doublon excitation tunneling into the leads. This is confirmed by analyzing the change in double occupation from equilibrium $\delta D_i(\tau)$ (Fig. 4 c-d). Note that the doublon is “long lived”, as evidenced by the dynamics of the double occupation within the MI region as it reflects off the boundary. This is a consequence of the weak decay of the doublon for large U/t'' (Ref. 18).

Additionally, there are interesting effects in the spin-spin correlation, as shown in the $S(q, \tau)$ plots in Figs. 4 e-f. A clear splitting of the peak occurs as the doublon and holon excitations become separated within the MI, also seen in Fig. 3. More interestingly is the fact that this feature is enhanced for a finite chemical potential difference (Figs. 4-f), a consequence of having a stronger charge tunneling between the MI and the leads (i.e. stronger “doping”, as discussed in Sec. III C).

A closer look on the charge dynamics at the interface is presented in Fig. 5, which depicts the behavior of the added charge $\delta n_i(\tau)$ at sites on both sides of the interface. A weak odd-even modulation is present so only odd-numbered sites are shown for a meaningful comparison. The amplitude of the charge excitation decays as the “charge front” approaches the boundary. In addition, a reflection at the interface takes place for $\tau \sim \tau_r = 5.5$ in both cases.

We can estimate the MI-metal charge reflection by comparing the maximum amplitudes of $\delta n_i(\tau)$ at sites on each side of the interface. For $\Delta\mu = 0$ (Fig. 5-a), the maximum in δn_i drops from 0.315 for $i = 29$ (within the MI) to 0.071 for $i = 31$ (in the leads), giving $R \equiv (\max \delta n_{29} - \max \delta n_{31}) / \max \delta n_{29} = 0.7737$. The rela-

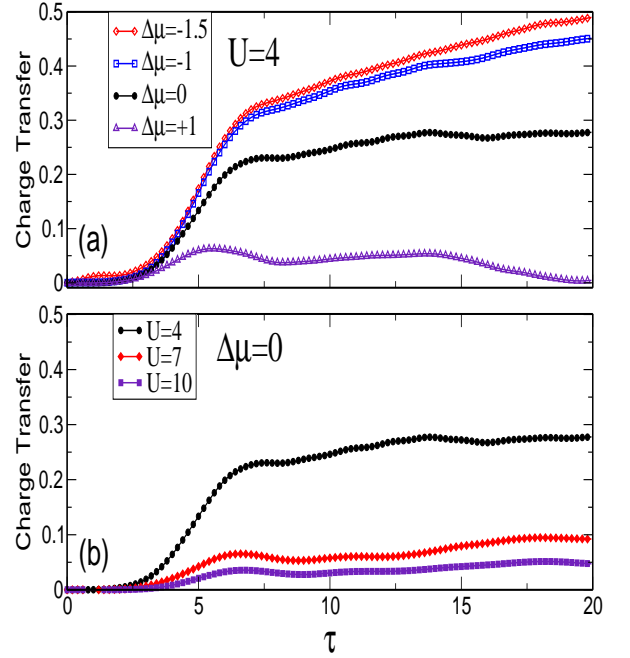


FIG. 6: Charge transfer (Eq. 3) for (a) $U = 4$ and different values of $\Delta\mu$ and (b) $\Delta\mu = 0$ and different values of U , with $t'' = 0.5$ in all cases.

tive drop is smaller for $\Delta\mu = -1$ (Fig. 5-b), with $R \approx 0.51$.

For longer times, further scattering of the doublon and holon excitations off the MI-metal interface result in additional charge tunneling into the leads. The integrated charge transferred to the right lead (Δn_R , defined in Eq. 3) is plotted in Fig. 6-a for different values of $\Delta\mu$. For longer times, $\Delta n_R(\tau)$ reaches an approximate plateau, indicating a steady state of the charge in the lead (for $\Delta\mu = -1.5$ the plateau has not been fully reached on the maximum time used in the calculations). As expected from our previous results, the height of the plateau is larger for negative values of $\Delta\mu$. For a stronger interaction U (larger Δ_{MI}), the charge transfer is strongly suppressed, as shown in Fig. 6-b.

These results indicate that the stronger the interaction U in the MI region, the more confined the holon-doublon pair becomes. This is clearly seen in Figs. 7(a,b) and (c,d), which depicts contour plots of $\delta n_i(\tau)$ and $\delta D_i(\tau)$ for $U = 4$ and $U = 10$, respectively. For $U = 10$, most of the charge remains confined in the MI region, reflecting off the interface in a periodic pattern. Interestingly, the long-lived holon and doublon excitations also “repel” each other, as seen for $\tau \sim 2\tau_r$.

Not surprisingly, increasing the Mott gap has a pronounced effect on the spin structure factor $S(q, \tau)$. Figs. 7-e and 7-f show $S(q, \tau)$ for $U = 4$ and $U = 10$, respectively. For $U = 4$, the three-peak structure (“shoulders”) disappear for $\tau \gtrsim \tau_r$, where a broad peak takes over. This is about the time scale for which the charge/spin fronts reach the boundary (Fig. 7-b). For $U = 10$, the shoulders reappear at later times, consistent with the “beating” in the doublon/holon pair as they reflect back and

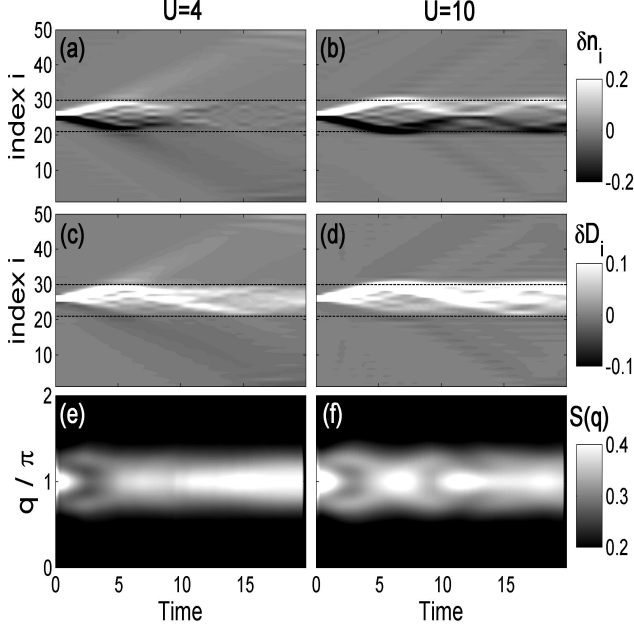


FIG. 7: Nonequilibrium charge $\delta n_i(\tau)$ (a,b) and double occupation $\delta D_i(\tau)$ (c,d) on each site as a function of time for $U = 4$ (a,c) and $U = 10$ (b,d). Panels (e,f) show the corresponding spin structure factor $S(q, \tau)$ in the MI region.

forth within the MI region and with each other. This is coupled with a much stronger confinement of the holon-doublon pair within the MI region, as seen in Figs. 7-b.

B. Comparison with the non-interacting case

An important question is how the results for the MI-leads charge transfer compare to a case where no electron-electron interactions are present in the central region. In order to address this question, we present results for two distinct cases: (i) a full “metallic” system, i.e., $U = V = 0$ and $t'' = 0.5$ in the H_{MI} term in Eq. 1 and (ii) a “band insulator” region, in which H_{MI} is replaced by

$$H_{\text{BI}} = -t'' \sum_{\sigma, i=N_L+1}^{N_L+N_{\text{MI}}} (1 + \delta(-1)^i) c_{i\sigma}^\dagger c_{i+1\sigma} + \text{h.c.} \quad (5)$$

in the Hamiltonian. Notice that H_{BI} represents a Peierls chain, which has a charge gap for $\delta \neq 0$ and the gap size will depend on t'' and δ . In the following, we choose $t'' = 1$ and $\delta = 0.6$ so that the band gap is nearly the same as the Mott gap for the case shown in Fig. 2-a ($U = 4$, $V = 0.3$, and $t'' = 0.5$).

Figures 8-a and b show the occupation $\langle n_i \rangle$ on the chain sites for the fully metallic and band insulator cases, respectively. The first case corresponds to the noninteracting limit of the results presented in the previous section, with a fully metallic chain. There are still strong reflections at the boundary due to the hopping mismatch

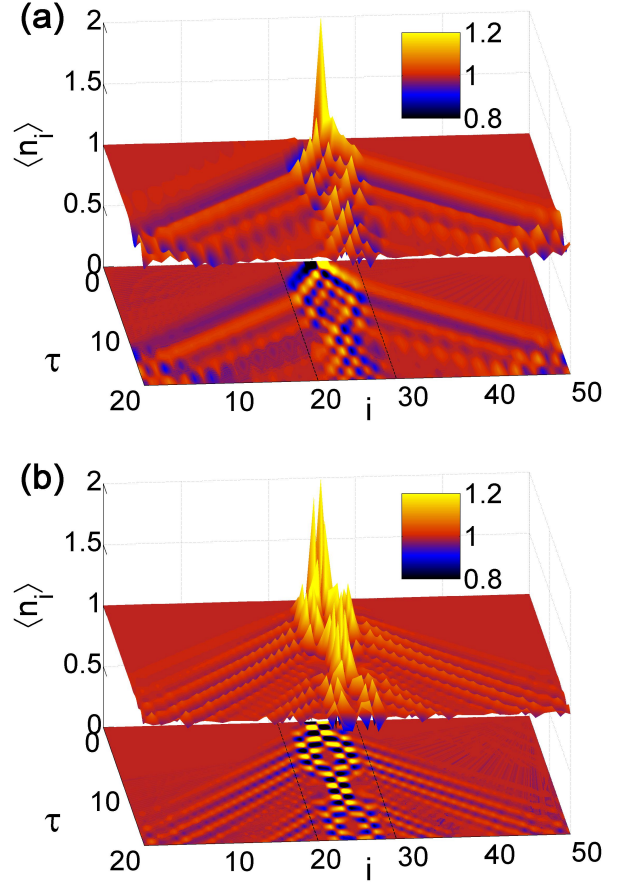


FIG. 8: Charge $\langle n_i \rangle$ on site i versus time τ for $N = 50$ sites, a non-interacting central region ($U = 0$), and $\Delta\mu = 0$. (a) is using a Hamiltonian as in Eq. 1 with $t'' = 0.5$ while in (b) H_{BI} replaces H_{MI} and $t'' = 1$, $\delta = 0.6$ (band insulator).

($t'' \neq t$). More importantly, the holon-doublon charge excitations produce Friedel-like oscillations along the chain, forming a clear charge interference pattern over time (see contour plot in Fig. 8-a).

For the case where the central region is a band insulator, charge oscillations also occur, leading to a “checkerboard” pattern of alternating positive and negative charges in the central sites (Fig. 8-b). In this case, propagation of a “charge wavefront” is clearly suppressed as compared to the fully metallic case.

The charge transfer to the right lead in both situations is clearly distinct from the interacting case. Figs. 9-a,b show a comparison of the charge transfer at $U = 4$ (same as depicted in Fig. 6) with results at $U = 0$ for $\Delta\mu = 0$ and $\Delta\mu = -1$, respectively.

The charge transfer is very limited for $\Delta\mu = 0$ in the noninteracting cases, having essentially a zero time-average for the band insulator. By contrast, the case $U = 4$ shows a positive transfer even for $\Delta\mu = 0$ due to the on-site repulsion within the central region. Note that the charge gap in the central region is nearly the same for both the Mott and band insulator cases, while

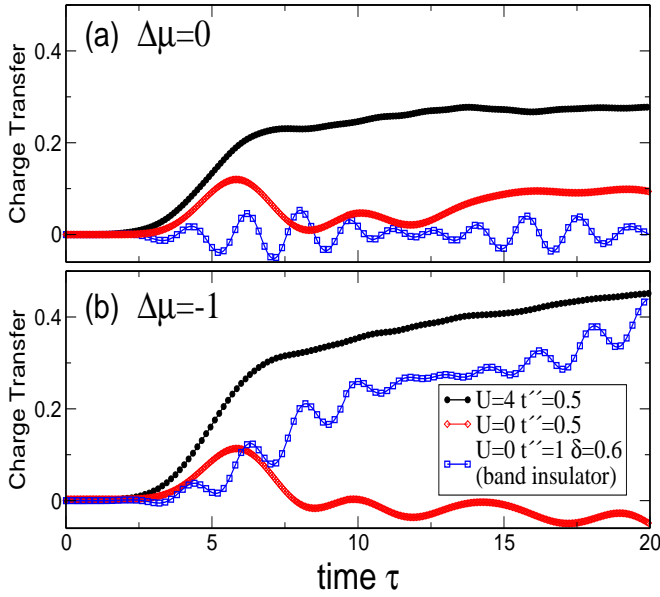


FIG. 9: Charge transfer comparison between the cases of interacting $U=4$ and noninteracting $U=0$ central regions, at two chemical potential differences. Results are also shown for a band insulator (Peierls chain) with a gap very similar to that of the Mott insulator with $U=4$.

the reflection at the boundary is much more accentuated for the latter. This highlights the role of the electron-electron interactions in the additional charge transfer for the $U = 4$ case.

For $\Delta\mu = -1$ (Fig. 9-b) the charge transfer is improved in the noninteracting cases, as expected. Overall, the charge transfer is still more effective in the case where the central region is a Mott insulator, as compared to the noninteracting cases.

C. Phase shifts in $S(q)$

In order to understand the three-peak feature in the spin structure factor, we have calculated $S(q)$ for a Hubbard chain with $N_L = N_R = 0$ and $N_{\text{MI}} = 40$ sites using static DMRG. We performed several DMRG calculations targeting states with different number of electrons N and total spin projection S_z . More specifically, we considered half-filling ($N = N_{\text{MI}}$) and hole-doped ($N = N_{\text{MI}} - N_h$ where N_h is the number of holes) cases, with $S_z = 0, 1/2$, and calculated the corresponding $S(q)$ for the different situations.

Results are presented in Fig. 10. For $N_h = 0$ and $S_z = 0$, the state corresponds to the antiferromagnetically ordered ground-state of the system at half-filling, with a peak at $q = \pi$. We then targeted states with different values of N_h and S_z . This corresponds to calculating the ground-state of a system in which holes and/or spin flips are added. For $N_h = 1$, $S_z = 1/2$ (one hole) and $N_h = 2$, $S_z = 0$ (two holes) a double peak structure appears.

This is reasonable since holons will introduce anti-

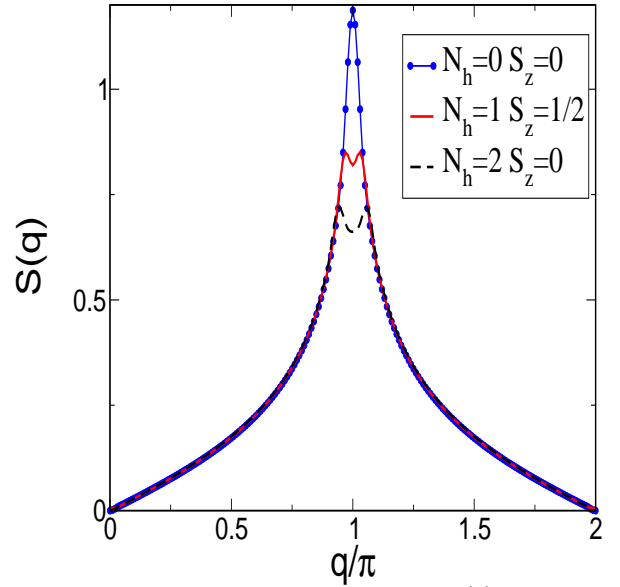


FIG. 10: Equilibrium spin structure factor $S(q)$ for a MI-only chain with N sites (no leads) calculated for states with charge $N - N_h$ (N_h is the number of holes) and spin S_z . Parameters are $U = 4$ and $t'' = 0.1$.

phase domain walls (ADW) (i.e. “ π -shifts”) in the AFM order and peaks at $\pi \pm \pi\nu_h$ are expected (where ν_h is the hole density). As spin-flips are added (for instance, $N_h = 1$, $S_z = 3/2$ the double-peak becomes four peaks (not shown). In light of these static calculations, the appearance of “shoulders” in $S(q, \tau)$ for $\tau < \tau_r$ (where τ_r is the time it takes for the excitations to reach the boundaries) can be accounted for as follows.

The creation of the holon/doublon pairs at $\tau = 0$ effectively removes two magnetic moments from the MI region, making $S_{p(p+1)}^z = 0$ at the holon (doublon) site. This explains the decrease in the area under the $S(q, \tau)$ curve at $\tau = 0$ as $\int S(q, \tau) dq \propto \sum_{i \in \text{MI}} \langle (S_i^z)^2 \rangle(\tau)$. For small τ , $S(q, \tau)$ still retains a single-peak structure initially since holon and doublon are on adjacent sites and the corresponding phase shifts from ADWs cancel out.

For $\tau < \tau_r$, the MI region can be divided into two parts with magnetically distinct characteristics: (i) an “undoped” region where neither the doublon or holon excitations have arrived and which still retains AFM order and (ii) a “doped” region, which has been already “covered” by either the doublon or the holon excitations. Part (i) contributes to a peak at $q = \pi$ in $S(q, \tau)$ while part (ii) contributes to the two shoulders, as we expect from the static calculations shown in Fig. 10 with $N_h = 2$.

For $\tau \sim \tau_r$, the excitation (and the corresponding ADW) reaches the boundaries, making the phase shifts to cancel out again, suppressing the side peaks. As the holon and doublon reflect off the boundaries, the side peaks reappear up to time scales of order $\tau \sim 2\tau_r$. At this time scale, doublon and holon excitations are again at nearest-neighbor sites and the respective ADW phase-shifts cancel once again, leading to a single-peak struc-

ture. The process then repeats up to time scales of the order of the doublon decay time thus this cycle is observed more clearly for larger values of U (e.g., Fig. 2-f) for which the doublon decay time is large enough. Notice that $S(q, \tau \sim 2\tau_r)$, although featuring a single peak at $q = \pi$, has a much smaller area than $S(q, \tau = 0)$, indicating that the propagation of the holon-doublon pair significantly modifies the AFM correlations.

IV. SUMMARY

In summary, we have studied the real-time propagation of doublon-holon excitations in a Mott insulator (MI) connected to metallic leads. We analyze the dynamics of charge, double occupation, and spin-spin correlations within the MI, as well as the MI-leads charge transfer.

Our results indicate that a sharp change in the Hamiltonian at the MI-metal interface hinders the charge transfer, suggesting that metals that closely resemble the structure of the MI¹⁶ would be required as charge collectors instead of standard doped semiconductors. More specifically, we find that the charge transfer across the MI-metal boundary is quite sensitive to microscopic parameters in the MI region, particularly the on-site interaction U . While U needs to be sufficiently large so that the doublon decay-time is larger than the typical time scale it takes to reach the boundary, doublon-holon tunneling into the leads is suppressed for very large values of U .

We believe two factors contribute to these results: (i) the increase of the Mott gap and (ii) the fact that, for large U , the nature of the doublon and holon excitations within the MI becomes more different than standard electron and hole excitations in the noninteracting case. We have tested these hypothesis by comparing configurations with either a Mott insulator or a (noninteracting) band insulator in the central region: they show clear differences in the charge transfer.

The repulsive interaction within the Mott insulator region favors the transfer of the excess charge into the metallic leads even at a zero chemical potential difference. This is in sharp contrast with a noninteracting band insulator connected to leads with the same band-

gap for which the net charge transfer is essentially zero at zero bias.

Noninteracting and interacting cases show clearly distinct charge dynamics after the excitation. In the former case, Friedel-like charge oscillations in the central region are prominent at small times, while they are suppressed in the interacting case and a clear spatial separation between hole-like and particle-like excitations occurs.

Moreover, the propagation of holons and doublons within the MI region dynamically alters the AFM spin-spin correlations. In particular, extra “ π shifts” appear in the spin correlation functions as doublons and holons are spatially separated. We believe these qualitative findings will help on the prospect of making future solar cell devices using strongly correlated materials.

An interesting aspect that remains open is the effect of a finite temperature in our results, a difficult problem considering that the numerical study of transport in correlated systems at finite temperatures remains a very challenging subject. The energy scales of spin and charge excitations in 1D Mott insulators can be quite different ($\sim t''$ for gapped charge excitations and $\sim (t'')^2/U$ for gapless spin excitations) and finite temperatures can affect each of these channels differently.^{25,26} In our case, however, since the doublon-holon pairs decay very weakly into spinon modes and the dynamics is governed by charge excitations, we expect the results to hold as long as temperatures are small compared to the charge gap.

Acknowledgments

We acknowledge motivating discussions with Ivan Gonzalez, Fabian Heidrich-Meisner, and Hiro Onishi. Research performed at the Materials Science and Technology Division, sponsored by the Division of Materials Sciences and Engineering, U.S. DOE, under contract with UT-Battelle, LLC. Computational support was provided by the National Energy Research Scientific Computing Center (NERSC). Work at LANL was carried out under the auspices of the NNSA of the U.S. DOE under Contract No. DE-AC52-06NA25396. LGGVDS and ED acknowledge support from NSF via grant DMR-0706020.

¹ Y. Tokura and N. Nagaosa, *Science* **288**, 462 (2000).

² W. Barford, *Phys. Rev. B* **65**, 205118 (2002).

³ E. Jeckelmann, *Phys. Rev. B* **67**, 075106 (2003).

⁴ H. Matsueda, T. Tohyama, and S. Maekawa, *Phys. Rev. B* **71**, 153106 (2005).

⁵ K. W. Kim, G. D. Gu, C. C. Homes, and T. W. Noh, *Phys. Rev. Lett.* **101**, 177404 (2008).

⁶ A. Gössling, R. Schmitz, H. Roth, M. W. Haverkort, T. Lorenz, J. A. Mydosh, E. Müller-Hartmann, and M. Grüninger, *Phys. Rev. B* **78**, 075122 (2008).

⁷ Y. Matiks, P. Horsch, R. K. Kremer, B. Keimer, and A. V.

Boris, arXiv:0909.5157 (2009).

⁸ I. Bloch, J. Dalibard, and W. Zwerger, *Rev. Mod. Phys.* **80**, 885 (2008).

⁹ C. Kollath, A. Iucci, T. Giamarchi, W. Hofstetter, and U. Schollwöck, *Phys. Rev. Lett.* **97**, 050402 (2006).

¹⁰ R. Joerdens, N. Strohmaier, K. Guenther, H. Moritz, and T. Esslinger, *Nature* **455**, 204 (2008).

¹¹ S. D. Huber and A. Rüegg, *Phys. Rev. Lett.* **102**, 065301 (2009).

¹² R. Sensarma, D. Pekker, M. D. Lukin, and E. Demler, *Phys. Rev. Lett.* **103**, 035303 (2009).

- ¹³ A. Rosch, D. Rasch, B. Binz, and M. Vojta, Phys. Rev. Lett. **101**, 265301 (2008).
- ¹⁴ F. Heidrich-Meisner, S. R. Manmana, M. Rigol, A. Muramatsu, A. E. Feiguin, and E. Dagotto, Phys. Rev. A **80**, 041603(R) (2009).
- ¹⁵ N. Strohmaier, D. Greif, R. Jordens, L. Tarruell, H. Moritz, T. Esslinger, R. Sensarma, D. Pekker, E. Altman, and E. Demler, arXiv:0905.2963 (2009).
- ¹⁶ H. Kishida, H. Matsuzaki, H. Okamoto, T. Manabe, M. Yamashita, Y. Taguchi, and Y. Tokura, Nature (London) **405**, 929 (2000).
- ¹⁷ H. Kishida, M. Ono, K. Miura, H. Okamoto, M. Izumi, T. Manako, M. Kawasaki, Y. Taguchi, Y. Tokura, T. Tohyama, et al., Phys. Rev. Lett. **87**, 177401 (2001).
- ¹⁸ K. A. Al-Hassanieh, F. A. Reboredo, A. E. Feiguin, I. González, and E. Dagotto, Phys. Rev. Lett. **100**, 166403 (2008).
- ¹⁹ C. Kollath, U. Schollwöck, and W. Zwerger, Phys. Rev. Lett. **95**, 176401 (2005).
- ²⁰ T. Ulbricht and P. Schmitteckert, Europhys. Lett. **86**, 57006 (2009).
- ²¹ U. Schollwöck, Rev. Mod. Phys. **77**, 259 (2005).
- ²² K. A. Hallberg, Adv. Phys. **55**, 477 (2006).
- ²³ S. R. White and A. E. Feiguin, Phys. Rev. Lett. **93**, 076401 (2004).
- ²⁴ A. J. Daley, C. Kollath, U. Schollwöck, and G. Vidal, J. Stat. Mech.: Theory Exp. **2004**, P04005 (2004).
- ²⁵ G. A. Fiete, Rev. Mod. Phys. **79**, 801 (2007).
- ²⁶ B. I. Halperin, J. Appl. Phys. **101**, 081601 (2007).